Smart dynamic rotor control: Part 1, Design of a smart rotor.

Teun Hulskamp*
a.w.hulskamp@tudelft.nl

Henri Champliaud**
henri.champliaud@etsmtl.ca

Jan-Willem van Wingerden*
j.w.vanwingerden@tudelft.nl

Thanasis Barlas*
t.barlas@tudelft.nl

Harald Bersee*
h.e.n.bersee@tudelft.nl

Gijs van Kuik*
g.a.m.vankuik@tudelft.nl

Michel Verhaegen*
m.verhaegen@tudelft.nl

*DUWIND, Delft University of Technology, Delft, The Netherlands
**Department of Mechanical Engineering, ETS, Montreal, Canada

Abstract

An important issue in researching the smart rotor concept is the load spectrum under investigation. In order to obtain a representative load spectrum in experiments on a small rotor, blades are designed of which the dynamic behaviour is scaled with respect to the rated rotational frequency. The blade design is also analyzed for stiffness, laminate strength and skin wrinkling because the design is fairly critical. The blade dynamics are analyzed using modal analysis.

Subsequently a series of blades is fabricated. The stiffness and dynamic results of the model are verified in experiments. Macro Fiber Composites (MFC) sensors are selected as the main strain sensor on which feedback control is based. The placement of the sensors is determined by performing a harmonic analysis.

The blades are mounted to a small turbine in the Delft University of Technology's Open Jet Facility (OJF) wind tunnel. The resonance peak associated with the first flapping mode lies exactly on the target 24Hz. Controllers are designed based on a measured state space model.

Finally, the rotor is employed in the jet and initial experiments with and without the controllers activated, are performed to show that the load spectrum as well as the performance of the system is what was aimed for in design. The observed load spectrum is as intended, with 1 and multiple-P spikes and a clear interaction between multiple-P loads and the blade's first flapwise mode. Also, with controllers active, a large reduction of the load spectrum is observed.

Keywords: Smart rotor, Design, Fatigue load reduction

1 Introduction

Today, fatigue loads are one of the most important design drivers for wind turbines. Moreover, with ever increasing turbine sizes these loads will increase even more, for instance because of gravitational loading and increased wind shear experienced by larger turbines.

Reducing the fatigue loading could lead to lighter blades or a longer service life of turbine components. Controlling turbine loads is therefore becoming more important. One of the fatigue load reduction concepts under investigation is the smart rotor concept. With the smart rotor concept, spanwise distributed devices are implemented to control the lift and drag characteristics along the span of the blade. In the last decade several studies of the concept have been made. See [1], [2], [3], [4] and [5].

Here, we present design and sample results of aero-elastic experiments on a small turbine equipped with trailing edge flaps. The flaps are controlled by a feedback controller which computes an actuation signal based on the deformations of the blade. After all, the fluctuations in blade root strain are to be minimized to minimize fatigue.

Table 1: Scaling parameters of the scaled turbine with respect to the reference turbine

Parameter	URT	Scaled rotor
Rated wind speed (m/s)	11.4	10
Tip speed ratio (-)	7	5
Rated rotational speed (rpm)	12	430
First mode (Hz) (flapwise bending)	0.69	24

$$f_{model} = \frac{f_{URT}\omega_{model}}{\omega_{URT}} \qquad (1)$$

In this f is the frequency of the first flapping mode and ω the rotational frequency. The subscript indicates whether the parameter relates to the scale model or the URT. See Table 1 for the scaling parameters.

The blade's design consists of a glass-epoxy laminate, wrapped around a solid core, which was infused using Vacuum Assisted Resin Transfer Moulding (VARTM) in a double rigid mould. The core mainly consists of a dense, 200kg/m^3, Airex C70.200 foam (Airex AG, Sins, Switzerland). At the base of the blade a steel insert is assembled with the foam to form a load introduction point at the blade-hub interface.

The blade is aerodynamically designed using a Blade Element Momentum (BEM) optimizer. It calculates the twist and chord, based on a given Tip Speed Ratio (TSR) and aerofoil data and iterates for optimal C_p. To successfully implement the actuators in the tip, a straight tip – without twist and taper - was desired. A DU96 W180 airfoil with a chord of 12cm was chosen for the tip. The same slender aerofoil was implemented along the whole span of the blade to obtain a flexible blade. The aerodynamic design does not lead to an optimal power conversion, but the goal of these experiments is to research the dynamic load reduction potential of the system, not optimal power conversion.

The Reynolds number at the tip is $2.4 \cdot 10^5$ which is relatively low, but neither Reynolds scaling, nor scaling to reduced frequencies is employed here.

The Finite Element (FE) model that is developed for the work described here is also used to provide input for the aero-elastic model described in part II. By validating the model in this series, we provide a tool for modelling similar 'smart' rotor systems on large MW-sized turbines. In part III the controller is discussed. The rotor, of which the design is discussed here, forms the physical system for which the controller is designed. However, in order to make the system representative of a 'real', full scale turbine the dynamics as well as the sensor and actuators have to be taken into account in the design process. This paper describes those design issues and the design process and through that presents a framework for smart rotor design.

2 Blade design and manufacturing

2.1 Conceptual design.

In order to research the feasibility of the smart rotor concept, a smart rotor was designed, manufactured and tested in a wind tunnel. The blade was dynamically scaled so that the ratio between the rotational speed and the blade's first eigenmode was the same as with the reference design, the UpWind 5MW Reference Turbine (URT) [6]. This is important because many of the disturbances are related to the rotation of the turbine, such as wind shear, tower shadow and yaw misalignment. These result in load fluctuations with mainly 1, 2 and 3P frequencies at the blade's reference frame. The blade's first flapping mode is close to the 3P frequency. By designing the blade such that the flapping frequency relates to the rotational frequency of the turbine, a realistic mix of rotationally induced disturbances and excited blade dynamics is obtained. Scaling is performed by using equation 1.

2.2 Structural analysis

A FE model is constructed in ANSYS [7] to optimize the number of skin plies to meet the strength, stiffness and dynamic requirements. The model consists of layered shell elements for the laminate and brick elements for the core part. When determining the geometry that is meshed, the thickness of the laminate is taken into account by defining a shape that corresponds to the core's geometry. The volume of the core is modelled with brick elements, and its outward surface is meshed with layered shell elements. The shape of the core has been computed in a way that when the laminate is added on its geometry, the external surface of the mesh coincides with the aerodynamic profile. This is done by giving a half thickness offset to the mid surface the shell elements

of the laminate. This is especially important near the blade root, where defining the steel root insert accurately is important for accurate predictions of the modes. The material properties are derived from previous tensile experiments. The loads are applied according to their definition in the BEM analysis; on the pitch axis.

The results of this analysis are that a skin of 2 plies which amounts to 0.5mm would be optimal. This leads to a frequency for the first (flapwise) eigenmode of 33Hz. See Figure 1.
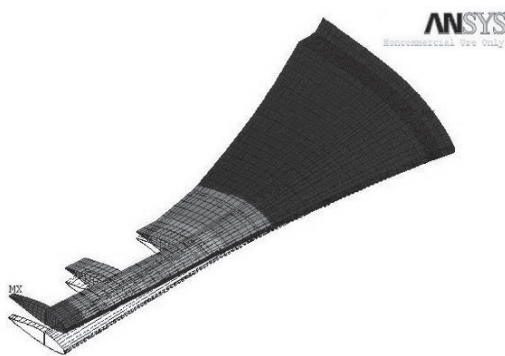

Figure 1: First flapping mode of the blade.

This is higher than the target frequency, but a linear modal analysis typically overestimates the eigenfrequency and in reality the blade fixation is also less stiff than modelled. Laminate strength is evaluated using a maximum stress criterion and laminate wrinkling is analysed using Plantema's criterion [8]:

$$\sigma = \frac{3}{2t_f} \sqrt[3]{2D_f E_C G_C} \qquad (2)$$

In which σ denotes the critical compressive stress in the facing. The subscript f indicates that it concerns the facing and c that it concerns the core. D is the bending stiffness of a laminate, E the Young's modulus and G the shear modulus. The criterion predicts whether a sandwich beam will wrinkle, depending on the elastic properties of the facings and the core. We can consider the blade as a whole as a sandwich beam, with the skin as the facing. A safety factor of 1 is used for the FE analysis, but when comparing the stress results of the FE model to the stresses of laminate failure and wrinkling, it is predicted that both stay well within the maximum allowable loads. See Table 2. The predicted wrinkling stress is 677MPa, which is well above both the

occurring stresses as well as the ultimate compression a stress.

Table 2: Occuring stresses and material strength.

	Max. occurring stresses	Material strength
Tension	31MPa	392MPa
Compression	24MPa	476MPa
Shear	14MPa	94MPa

2.3 Manufacturing and testing

Subsequently, a mould and core parts were milled to size. Holes were drilled through the steel and foam to fit the sensor and actuator cables as well as a safety cable. The straight outboard section was equipped with a glass-epoxy spar which acts as reinforcement and mounting point for the actuators where the flaps are installed. It is of paramount importance that the core shape is highly accurate and accurately assembled. Any deviating shape will lead to local high pressure on the laminate which leads to bad infusion and local dry spots.

After infusion and removal from the mould, superfluous resin is removed and two slots are cut out in the outboard section to fit the flaps. The flaps are based on piezo-electric Thunder actuators. Piezo-electric driven flaps are needed because an actuation bandwidth of about 100Hz is needed to control the dynamic loads that are associated with the major part of the load spectra – including the first edgewise mode which is left out of scope in these experiments, but which might be addressed in the future. The Thunder actuators are shaped with foam to match the shape of the profile and at the same time allow for the bending motion of the actuator.

The deflection of the flap is in the order of several millimetres for maximum actuation voltage. Knowledge about the exact deflection is not needed to analyse the performance of the system, because the controller, which is discussed in part III regards the system as a black box. However, before constructing the actual actuators in the blades, a prototype was constructed and tested to observe whether the flap deflection would be in the right range.

The blade is tested in a testing machine, both in static and dynamic excitation tests. A special jig is made to mount the blade to the testing machine and excite it at its flap locations. See Figure 2. In static testing 4% deviation in stiffness between the test and FE model for the same load case was found

Figure 2: Blade testing set-up

Figure 3: dynamic behavior of the stresses at the sensor location.

and no damage, nor change in stiffness was observed at the design load.

2.4 Sensor Placement

The control system is based on the blade's deformation. Different sensors are tested, viz. piezo electric ceramic based sensors, piezo electric polymer films and strain gages.

Placement of the strain sensors is determined by performing a harmonic analysis with the FE model. Through this analysis the strain magnitude and phase behaviour (sometimes referred to as 'delay' in the wind energy community) at different locations on the blade surface as a result of an excitation force can be derived.

The goal is to obtain so called collocated behaviour [9],[10]. With collocated control, the sensor and actuator are associated with the same degree of freedom of the system. This is obviously the case when a displacement transducer and actuator are placed at the same location. But in the case of vibration of a cantilevered beam which is measured by a strain sensor, the displacement at the actuator location is associated with a strain elsewhere. This relation, as a function of excitation frequency, can be determined with the harmonic analysis.

One of the features of a collocated sensor-actuator pair is that the when observing the Bode plots, the gain plot is characterized by alternating resonance and anti-resonance peaks. In the phase diagram this results in a phase lag between 0 and -180 degrees.

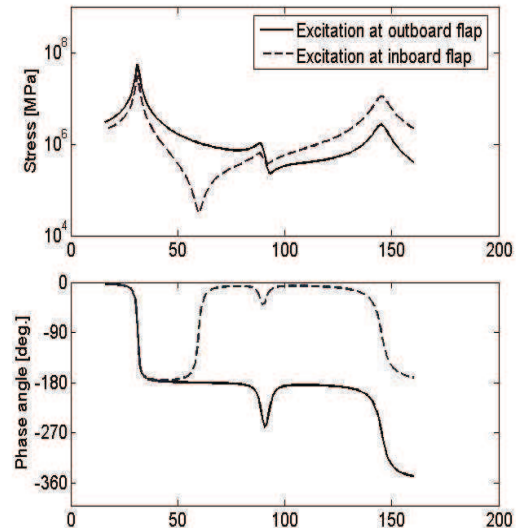As can be seen in the Figure 3, this is obtained for excitation at the inboard flap, but not for the inboard flap. However for the frequency range of interest the behaviour is acceptable.

In addition, accelerometers are mounted at the flap locations. The piezo electric ceramic sensors, called MFC's [11] provide the highest signal to noise ratio and also do not require any amplification. They are therefore selected as the primary sensor on which the feedback controller will act. Two MFC's are adhered: One on the pitch axis to measure the flapwise bending deformation and one on the leading edge to measure the edgewise bending moment. At the same location additional strain gages are adhered. The MFC electrodes are bridged by a high ohmic resistance and a capacitor so that effectively a high pass filter is created. Thus the static loads are filtered out and only load fluctuations are recorded. Moreover, at the flap locations, accelerometers are installed to measure edgewise and flapwise accelerations. In the experiments described here, the accelerometers are not used for control, but they are available for future experiments.

3 Wind tunnel set-up

A picture of the blades mounted to the rotor, with indication of the different components can be seen in Figure 4.

The rotor is placed in the tunnel's jet. The tunnel can only supply a constant airspeed, but the turbulence level is not very low. Due

to the open nature of the tunnel there are little or no wall effects. The test section is about 6m high and wide, whereas the jet has a diameter of 3m and the rotor diameter is only 1.8m. Part of the octagonal jet can also be seen in Figure 4.
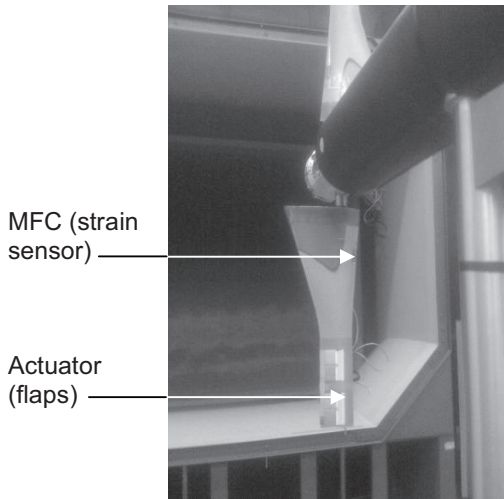

MFC (strain sensor)

Actuator (flaps)

Figure 4: Installed blades

Only two blades are installed, because the turbine only has the capability to have two blades mounted to it. Of course this is taken into account in the blade's (aerodynamic) design. The main difference relevant to these experiments is the sampling of multiple-P loads. The sampling of dynamic inflow is the same for any number of blades. But when the loads are transmitted through the hub, with a two bladed rotor 2 and 4P loads are more dominant, compared to 3P and 6P loads with three blades. But the effect is similar.

The all sensor and actuator signals are connected to the different control systems, as indicated in Figure 5. A dSpace system (dSPACE GmbH, Paderborn, Germany) is used to record the signals from the blade sensors and to control the flaps. A National Instruments LabVIEW system is used to provide a Graphical User Interface (GUI) for the turbine's controller which assures constant speed. Therefore the turbine control is completely separated from the flap control. The generator itself is a synchronous servomotor. The generator is connected to a dissipater to which electrical power can be fed that is converted from the wind when the system works as a turbine.

4 System performance

Multiple controllers were developed and implemented, aimed at the 1, 2, 3 and 4P as well as the first flapping mode. Details about the controller design can be found in part III of this series [12]. Here they are presented to show that the load control system works as intended. In Figure 6 the square root of the Power Spectral Densities (PSD) can be seen for a 5° yaw angle, without controller. The
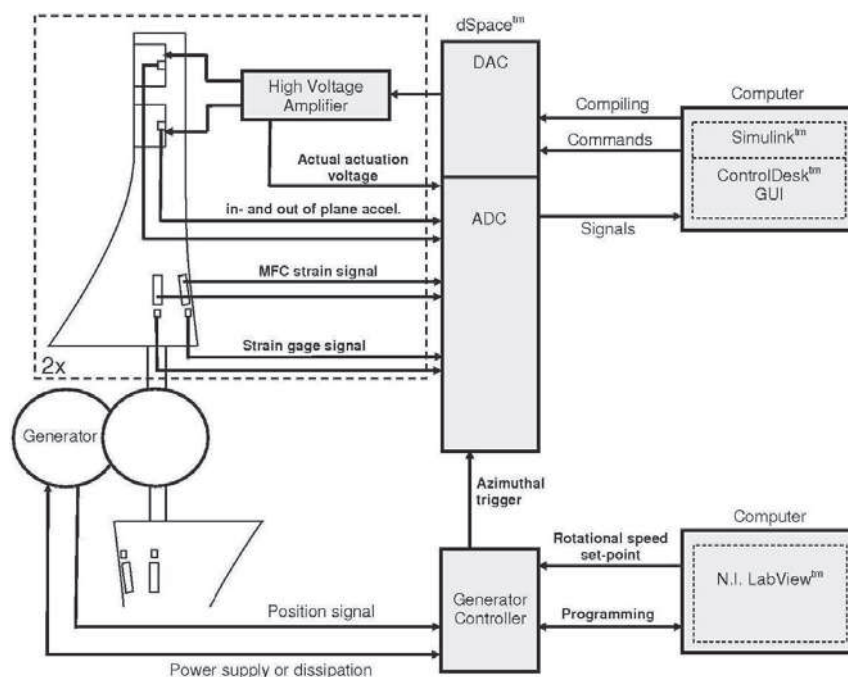

Figure 5: Control scheme of the smart rotor and the turbine.

resonance peak can be seen at 24Hz, as intended in design, as well as the 1P load spike and sampling of it at multiple-P frequencies. Although the results are for a case at which the turbine was rotating at 370rpm instead of the rated 430rpm, the interaction between the multiple P loads (4P in this case) and first flapping mode can clearly be observed. One would expect the 4P spike to be of same order as the 2P peak, but the proximity of the resonance peak amplifies the vibration. The generator unfortunately didn't allow testing at 430rpm at the time of the experiments discussed here. But the wind speed is changed accordingly, so rotating at 370rpm should be considered as a below-rated load case.

As an indication of the overall load reduction the relative standard deviation is presented in Figure 7. In this plot, the standard deviation of the respective series without controller equals 1:

$$\text{plotted value} = \frac{\text{std}_{\text{with controller}}}{\text{std}_{\text{without controller}}} \qquad (3)$$

The results with a H_∞ controller are presented. In all cases the loads are clearly reduced. See part III of this series for more details on the load reduction with different controllers.

5 Conclusions

In this paper we described the issues with designing a smart rotor for a wind turbine. A set of blades was designed manufactured and tested. With the test the FE model that was developed for design was validated and the performance of different sensors was tested. The load spectrum that was observed in wind tunnel experiments was as aimed for and the performance of the load control system is clearly shown.

The validated FE model discussed in this paper, provides input for the aero-elastic model which is discussed in part II of this series and which, in turn, is also validated with these experiments.

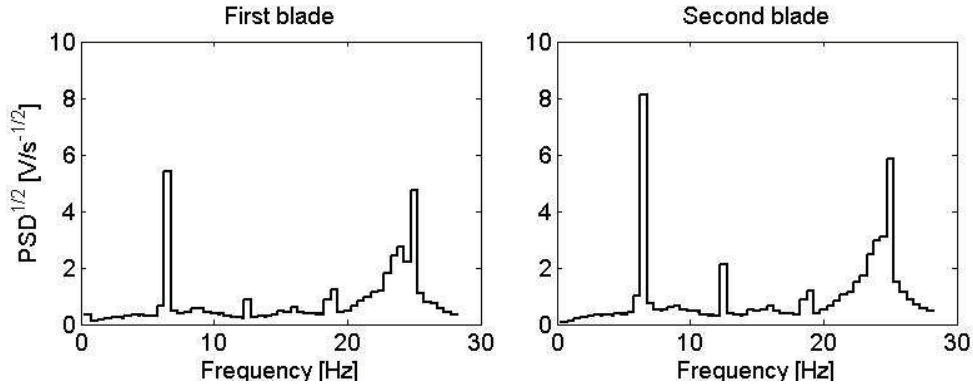Furthermore, through this work we provided a platform on which the feasibility of

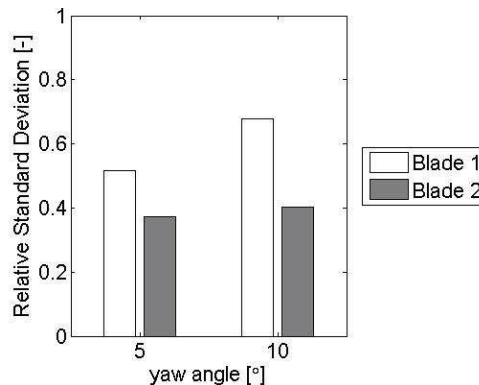Figure 6: PSD of the MFC signal for 5° yaw without control

Figure 7: Relative standard deviation of the time series for different yaw angles with a H_∞ controller.

the smart rotor system on a rotating machine was shown. As a matter of fact, the platform already provides key parts of the system in the form of actuators and sensors. In part III of this series, different controllers which use the sensors as inputs and control the flaps are discussed.

Finally, we have addressed key issues in the design of blades when they are to be 'smart' rotor blades, namely taking into account the dynamic behaviour of the blades and the sensor selection and placement. The actuators used in these experiments are not upscalable to full scale rotor designs because they take up over half the chord of the tip-profile. This is needed here, because of the small scale of the blades and the required actuator authority. For full scale blades it is asserted that 10-20% of the chord should suffice to obtain a similar performance.

References

[1] Andersen, P., Gauna, M., Bak, C. & Buhl, T., "Load alleviation on wind turbine blades using variable airfoil geometry", *Proceedings of European Wind Energy Conference and Exhibition, European Wind Energy Association*, Brussels, 2006.

[2] Joncas, S., Bergsma, O. & Beukers, A., "Power regulation and optimization of offshore wind turbines through trailing edge flap control", *Proceedings of the 43rd AIAA Aerospace Science Meeting and Exhibit*, 2005.

[3] Basualdo, S., "Load alleviation on wind turbine blades using variable airfoil geometry", *Wind Engineering*, Vol.29, 2005.

[4] Lackner, M.A. and van Kuik, G., "A comparison of smart rotor control approaches using trailing edge flaps and individual pitch control", *Wind Energy*, 2009, Published Online.

[5] Barlas, T. and van Kuik, G., "State of the art and prospectives of smart rotor control for wind turbines", *Journal of Physics: Conference Series*, Vol.75, 2007

[6] Jonkman, J., Johansen, J., Lindenburg, K., *et al. "Description of the UpWind Reference Wind Turbine"* – Version 9 – 2007.

[7] Release 11.0 Documentation for ANSYS, 2007, ANSYS Inc.

[8] Fagerberg, L., "Wrinkling and Compression Failure Transition in Sandwich Panels", *Journal of Sandwich Structures and Materials,* Vol. 6., 2004

[9] André Preumont, Vibration Control of Active Structures - An Introduction, Kluwer, 2004 (2nd edition)

[10] MacMartin, D., Collocated structural control: motivation and methodology. *Proc. of the 4th IEEE Conf. on Control Applications*, 1995

[11] Sodano, H., Park, S. and Inman, D. "An Investigation Into The Performance Of Macro-Fiber Composites For Sensing And Structural Vibration Applications", *Mechanical Systems and Signal Processing*, Vol.18, 2004.

[12] J.W. van Wingerden et al. "Smart Dynamic Rotor Control: Part3, advanced controller design", *Proceedings of The Science of Making Torque from Wind*, Heraklion, Greece, 2010